

Particle Dark Matter Constraints from the Draco Dwarf Galaxy

C. TYLER

Department of Astronomy & Astrophysics,
The University of Chicago, Chicago, IL 60637

Abstract. It is widely thought that neutralinos, the lightest supersymmetric particles, could comprise most of the dark matter. If so, then dark halos will emit radio and gamma ray signals initiated by neutralino annihilation. A particularly promising place to look for these indicators is at the center of the local group dwarf spheroidal galaxy Draco, and recent measurements of the motion of its stars have revealed it to be an even better target for dark matter detection than previously thought. We compute limits on WIMP properties for various models of Draco's dark matter halo. We find that if the halo is nearly isothermal, as the new measurements indicate, then current gamma ray flux limits prohibit much of the neutralino parameter space. If Draco has a moderate magnetic field, then current radio limits can rule out more of it. These results are appreciably stronger than other current constraints, and so acquiring more detailed data on Draco's density profile becomes one of the most promising avenues for identifying dark matter.

1 Introduction

Despite the popularity of the neutralino as a dark matter candidate, efforts to constrain its properties have only been able to rule out a small fraction of the relevant parameter space. Direct detection experiments based on scattering with nuclei, and indirect searches based on neutralino annihilation, have shared this difficulty. But recent results can improve the situation. New observations of the Draco dwarf galaxy reveal that it is strongly dark matter dominated, and that its dark matter distribution is at least nearly isothermal. In this paper we investigate the detectability of WIMP annihilation signals from several appropriate halo models. Interestingly, if Draco is indeed isothermal down to very small radii, we will show that current gamma ray measurements rule out a significant fraction of the neutralino parameter space. If one makes an additional assumption that Draco harbors magnetic fields, then current radio measurements rule out additional parameter space. For example, a $1 \mu\text{G}$ field would eliminate most of it. Other halo models yield weaker current limits, some of which become significant with upcoming detectors.

The choice of a particular dark matter distribution is critical to both gamma ray and radio limits, and we devote section 2 of this paper to that consideration. The assumption of a magnetic field in Draco is discussed in section 4. The remainder of this introductory section provides the relevant background.

The cold dark matter (CDM) scenario starts with a weakly interacting massive particle (WIMP), created abundantly in the big bang and surviving today to dominate the matter density in galaxies. The velocities of stellar orbits imply that dark matter occupies galaxies with a particular radial density profile. Over a wide range in radius, the density appears to fall off as $\rho \sim r^{-2}$, which is the same structure as would be found in a self-gravitating isothermal sphere. But when simulations of the cosmological CDM evolution are performed, taking into account the influence of N -body dynamics and tidal interactions, the profiles are found to be more complicated at large and small r (e.g., Navarro, Frenk, and White (1996), Moore et al. (1999)). We discuss these profiles in more detail in subsection 2.1.

Simulations universally generate a central cusp in every dark halo. Slopes vary, but $\rho \sim r^{-\gamma}$ remains for some positive γ , and therefore the density blows up at the center. However, a controversy ensues at this point because observations often differ. 21 cm rotation curves from low surface brightness (LSB) galaxies have presented evidence for central cores of approximately constant density (McGaugh and de Blok, 1998). A separate study of 16 LSB galaxies contends that beam smearing effects render these measurements unreliable, such that cusps are still fully consistent with the data (van den Bosch et al., 2000). Many of the same galaxies have since been re-examined with high resolution optical rotation curves, and that work found 30 LSB galaxies evidently possessing cores, not CDM cusps (de Blok, McGaugh, and Rubin, 2001). Dwarf galaxies too have long been considered problematic for CDM because they typically have the linearly rising rotation curves of a constant density core (Navarro, Frenk, and White, 1996), but a subsequent study of 20 dwarf galaxies gives rise to interpretations ranging from cores to steep r^{-2} cusps (van den Bosch and Swaters, 2001). These issues constitute an area of much debate, but in general, because many observations favor cores over cusps, it is of great interest to determine what processes might prevent or destroy a cusp.

If a WIMP cusp were to realize, and if WIMPs exist today in equal numbers with antiWIMPs (or if they are their own antiparticles), then we can expect densities high enough for dark matter annihilation to become significant. If the annihilation products lead to observable particles, then cusps become hot spots to search for WIMPs.

Perhaps the most likely WIMP candidate is the neutralino (χ), which is the lightest supersymmetric particle (LSP) in the minimal supersymmetric extension of the standard model.

Supersymmetry is a symmetry relating fermions to bosons, and thus it introduces a new class of particles which are “superpartners” to standard model particles. The theory helps to remedy the hierarchy problem set by the electroweak and Planck scales. In models with conservation of R-parity, a supersymmetric particle is prohibited from decaying into only non-supersymmetric ones, and since the neutralino is the LSP, there is no supersymmetric state of lower energy available. Thus the χ is stable, making it a well motivated dark matter candidate (for a review of supersymmetric dark matter, see Jungman, Kamionkowski, and Griest (1996)).

Each $\chi\bar{\chi}$ annihilation produces quarks which bind primarily into pions. Neutral pions usually decay to gamma rays; charged pions usually decay to neutrinos and muons, and subsequently electrons (and positrons), which generate radio waves by synchrotron radiation in an ambient magnetic field. (This approach does not wholly rely on supersymmetry, but rather on some DM particle which annihilates into pions.) Therefore, a cusp produces observable radio and gamma radiation (Berezinsky, Gurevich, and Zybin, 1992; Berezinsky, Bottino, and Mignola, 1994); the trick is just finding a galaxy with a cusp.

The candidate galaxy should have a very high mass-to-light ratio (M/L) to ensure that its internal gravitation is DM dominated, and it should be nearby to facilitate the detection of a weak signal. As it turns out, the highest known M/L comes from a dwarf satellite of our own Galaxy. The Draco dwarf spheroidal galaxy, only 79 kpc distant from Earth (van den Bergh, 2000), was recently re-examined for detailed stellar velocities (Kleyna et al., 2001a). A new, higher than previously estimated M/L was found to be $440 \pm 240 M_{\odot}/L_{\odot}$, with a mass of $M \simeq 8.6 \times 10^7 M_{\odot}$. Draco has the mass of a dwarf galaxy and the starlight of a globular cluster.

Furthermore, the candidate galaxy should have a high central WIMP density, without contaminants such as massive baryonic clouds or a central black hole. The stellar velocity dispersion measurements in Draco are consistent with an isothermal dark matter halo (Kleyna et al., 2001a), implying a steep central density. Its present hydrogen gas population is less than $450 M_{\odot}$ (Young, 1999), with no evidence of a central black hole. The Sloan Digital Sky Survey reported that tidal deformation can only exist at a level of $\leq 10^{-3}$ of the central stellar surface density (Odenkirchen et al., 2001), supporting the case for dynamical relaxation and therefore meaningful extraction of mass density from velocity information. Given these properties, we present particle dark matter constraints enabled by observations of the stars in Draco.

The next section provides more detail regarding halos with cusps and cores. Section 3 follows with the calculation of the observable flux created by WIMP annihilations, including electron losses by inverse Compton scattering, which is an important correction not usually considered in such analyses. Section 4 presents the results of these calculations, using observational bounds from EGRET and the VLA, with a discussion of anticipated improvements by new experiments, and a comparison among various halo profiles. We summarize in section 5.

2 The Dark Halo

A power law cusp’s density profile has the form $\rho \sim r^{-\gamma}$. Binney and Tremaine (1987) have put forth some reasoning for the expectation of a singular isothermal sphere (SIS) distribution to a first approximation, where $\gamma = 2$. But do steep cusps like this really exist in nature?

Observations of galaxy centers with the Hubble Space Telescope (HST) shed some light on this question (Crane et al., 1993; Gebhardt et al., 1996). These authors have constructed three dimensional luminosity densities based on an assumed spherical geometry in the target ellipticals and in the bulges of spirals, further assuming that the light traces the mass in these systems. Among power law galaxy centers, two populations emerge: bright galaxies (roughly $M_V \leq -20$) with slopes in the range $0.2 \leq \gamma \leq 1.5$, and faint galaxies ($M_V \geq -20$) with γ ranging between $1.5 \leq \gamma \leq 2.5$. The peaks in this bimodal distribution are at 0.8 and 1.9, respectively. Many faint galaxies in the sample therefore have nearly isothermal density profiles at their centers.

2.1 Halo Models

An ordinary kinetic-molecular gas, self-gravitating and held isothermal, will assume the SIS density profile $\rho \sim r^{-2}$. Instead, we have a collisionless system of WIMP particles. If they are allowed to evolve under their collective gravitational potential, the initial infall can be expected to be clumpy, and as a result, the overall potential seen by any one WIMP is the superposition of the central field and the temporary groupings. Trajectories are thus altered, and over a few orbital periods, a new smooth centrally weighted distribution will be obtained. This process was termed “violent relaxation” by its author, Lynden-Bell (1967), wherein the central collapse is achieved by transporting angular momentum outward.

The solution at the end of this relaxation turns out to be the Maxwellian velocity distribution with constant velocity dispersion at every radius, although the population dwindles somewhat beyond the virial radius, as those particles do not often interact with the lumpy center and therefore do not join the infall. One important caveat, however, is that the violent relaxation process proceeds until a steady state is achieved, whether or not that state is the Maxwellian result of complete relaxation. This means that it is possible for the final state to retain features unique to its own collapse sequence (one reason why simulations are useful for this work).

Supposing the end state of the process is complete relaxation, we have a system of self-gravitating particles with a Maxwellian velocity distribution at every point in space, the solution of which is again the SIS density profile (Binney and Tremaine, 1987). If the system fails to achieve complete relaxation, then the innermost orbits may not be fully populated, and one might expect $\gamma < 2$ as is often seen in numerical simulations.

Rotation curves of galaxies usually show a constant velocity over a wide range of radial values. On the contrary however, some observations reveal core regions of about 1 –

10 kpc in radius which appear to enclose an r -independent matter density. This is evident in the rotation curves of spiral galaxies which tend to rise linearly at small radii, and those of some dwarf galaxies which rise linearly for the full extent of the observed galaxy. To model this, one typically invokes a modified isothermal profile: a spherically symmetric density profile which smoothly blends a constant density core with isothermal behavior outside the core.

In order to calculate observables from annihilation reactions, one must start by assuming some profile. For example, gamma rays from annihilating neutralinos were originally calculated by Berezhinsky, Gurevich, and Zybin (1992) using $\rho \sim r^{-1.8}$ for the Galactic center. In Gondolo (1993), the same signature from the Large Magellanic Cloud was calculated assuming $\rho \sim a^2/(r^2 + a^2)$, a modified isothermal model with core radius a . Non-constant central densities with radial power law exponents have been employed in different contexts: $\gamma = 1$ (NFW: Navarro, Frenk, and White (1996), used for example in Gondolo (2000) and Blasi, Olinto, and Tyler (2002)), $\gamma = 1.5$ (Moore: Moore et al. (1999), used for example in Calcáneo–Roldán and Moore (2001)), and $\gamma = 2$ (isothermal: used for example in Blasi, Olinto, and Tyler (2002)). It is worth mentioning that γ appears to vary with the resolution of the CDM simulation, and at small radii, a realistic model of the high cusp density can be expected to require more accurate simulations.

In this work, we consider seven distinct models of Draco. These include steep power-law cusps with $\gamma \leq 2$, the Moore profile, and isothermal halos truncated by constant density cores.

A power law DM halo profile must include a small constant density core inside the cusp for any $\gamma > 0$, due to the fact that inside some radius, the annihilation rate gets so large that the over-density is destroyed as fast as new infall can fill the region. The constant density region, found by setting cusp forming time scale (the clump crossing time, or approximately the free fall time $\sim 1/\sqrt{G\rho}$) equal to the annihilation time scale ($1/n_\chi \langle \sigma v \rangle_{\chi\bar{\chi}}$), establishes a characteristic inner radius (Berezhinsky, Gurevich, and Zybin, 1992). For example, if $\gamma = 2$ (SIS), we have (Blasi, Olinto, and Tyler, 2002):

$$R_{\min} = R_{\text{ext}} \langle \sigma v \rangle_{\chi\bar{\chi}}^{\frac{1}{2}} \left[\frac{n_{\text{halo}}}{4\pi G m_\chi} \right]^{\frac{1}{4}}, \quad (1)$$

where the $\chi\bar{\chi}$ annihilation rate (cross section \times velocity) $\langle \sigma v \rangle_{\chi\bar{\chi}}$ is approximately constant in the low velocity limit appropriate for galactic dark matter (Berezhinsky, Gurevich, and Zybin, 1992), and the time scales mentioned above are $\sim 5 \times 10^8$ years at R_{\min} . The external radius R_{ext} of Draco’s halo is where it blends smoothly into the Milky Way halo. If we define the cuspy halo density as

$$n_\chi = A r^{-\gamma}, \quad (2)$$

then R_{ext} and the coefficient A can be jointly set by equating the χ density at the edge of Draco’s halo to the ambient Milky Way halo density at Draco’s location, n_{halo} . Additionally, integrating eq. (2) out to R_{ext} must give Draco’s total

mass. The following are numerical values for these quantities, taking $m_\chi = 100$ GeV and $\langle \sigma v \rangle_{\chi\bar{\chi}} = 10^{-26}$ cm³/s, listed here for the $\gamma = 2$ case (the generalization to $\gamma < 2$ is straightforward):

$$\begin{aligned} R_{\text{ext}} &= 4.6 \text{ kpc} \\ R_{\min} &= 9.4 \times 10^{14} \text{ cm} \\ n_{\text{halo}} &= 2.2 \times 10^{-5} \text{ cm}^{-3} \\ n(R_{\min}) &= 5.7 \times 10^9 \text{ cm}^{-3}. \end{aligned}$$

As will be discussed in subsection 3.1, the gamma ray flux observed from a DM clump depends on R_{\min} , so it is worth considering whether it is appropriate to use the free fall time as the cusp formation time. Since violent relaxation is a complex process one might imagine some longer characteristic time scale. Without any particularly compelling choice for this time scale, we can set a conservative upper limit by using the age of the universe. For Draco, using $\tau_{\text{univ}} = 15$ Gyr, the resulting gamma ray flux is found to be about 5 times weaker than it would be with eq. (1), for any choice of m_χ .

The NFW and Moore halo profiles mentioned previously are the most popularly quoted “universal profiles” obtained from simulations. Both employ power-law cusps internal to some scale radius, outside which the density falls off as r^{-3} . The behavior is nearly isothermal in the vicinity of the scale radius r_s .

In calculating R_{ext} , we have used the customary NFW profile for our own Galaxy,

$$n_{\text{halo}} = n_0 \left(\frac{r}{r_s} \right)^{-1} \left[1 + \frac{r}{r_s} \right]^{-2}, \quad (3)$$

whose scale radius $r_s \simeq 30$ kpc, total size $R_{\text{ext}} \simeq 300$ kpc, and characteristic density $n_0 \simeq 7.5 \times 10^{-4}$ cm⁻³, can be set by the boundary conditions imposed by the halo density local to our solar system (6.5×10^{-25} g/cm³), and the total mass of the Galaxy ($10^{12} M_\odot$), subject to an estimate that $R_{\text{ext}}/r_s \simeq 10$. As it turns out, various Galactic halo models roughly agree on the local dark matter density at Draco’s distance from the center, so the choice of NFW as the Milky Way DM profile is not particularly important here.

The Moore profile (Moore et al., 1999) is more recent, deriving from higher resolution computations than NFW. We therefore include it in our calculations of Draco. The Moore profile is

$$n(r) = n_0 \left(\frac{r}{r_s} \right)^{-1.5} \left[1 + \left(\frac{r}{r_s} \right)^{1.5} \right]^{-1}, \quad (4)$$

where $n_0 \simeq 2.5 \times 10^{-2}$ cm⁻³ and $r_s \simeq 0.35$ kpc can be fixed in similar fashion, using Draco’s total mass, the Milky Way density local to Draco, and a concentration factor $R_{\text{ext}}/r_s \simeq 10$ as boundary conditions.

In a recent paper (Power et al., 2002), a convergence study is described which attempts to resolve central halo densities in CDM simulations. The result for a galaxy-sized halo appears to be a decreasing exponent moving inward from

the virial radius (comparable to R_{ext} in this work), reaching $\gamma \leq 1.2$, without any particular inner power law slope convergence. Because this is a state-of-the-art simulation, the fact that the inner slope is not especially steep should not be ignored. However, the authors note that their innermost resolved point is only 0.5% of the virial radius, which is outside our region of interest for Draco, and that the effect of poor resolution is usually to generate artificially low central densities. The reasons which cause this simulation to differ in inner slope from others like Moore are currently unclear, but external to a few times the innermost resolved radius, the various CDM halo profiles are difficult to distinguish. In any case, the central drop in γ is not evident in Draco.

2.2 Modeling Draco

The stellar motion measurements from Draco are best fit by $\gamma \simeq 1.7$ over ~ 1 kpc (Kleyna et al., 2001a); strong velocity anisotropies and strong deviations from isothermality are ruled out over this radial scale. (Star counts and luminosity density are insufficient for determining the mass profile, because according to the same stellar velocity study, mass does not follow light in Draco.) In the central ~ 0.2 kpc, γ appears to be ≥ 2 , although other cusp slopes and cores cannot be ruled out at small radii with the current data set. So although the observations support the SIS at intermediate radii, they don't directly speak for radii smaller than about 10 pc, inside which our annihilation signal originates.

Since annihilation rate goes as the square of the density of χ particles ($n_{\chi}^2 \langle \sigma v \rangle_{\chi\bar{\chi}} \text{ cm}^{-3} \text{ s}^{-1}$), the choice of γ is very important to the result. Observed γ values from rotation curves are neither accurate enough nor consistent enough to use uniformly for this purpose. Although a positive detection of gamma or radio signals could identify a particle dark matter source, the difficulty in choosing γ with any confidence has made it hard to realistically constrain WIMP parameters such as mass and cross section on the merit of observational upper limits alone.

However, this situation may soon change. Draco's mass has recently been shown to be completely dominated by dark matter, with stellar velocities that favor nearly isothermal organization, and the authors of these observations contend that the prospects are excellent for improving the velocity curve data further by sampling more stars (Kleyna et al., 2001a). This may become a particularly fruitful approach to further particle DM studies. So to agree well with current data on Draco, we use halo models with $\gamma = 2.0, 1.9, 1.8$, and 1.7 , the Moore profile, and isothermal profiles truncated with cores at 1 pc and 0.1 pc.

Other galaxies currently have more detailed velocity dispersion or rotation data. We choose Draco for this study partly for its proximity, and partly for its lack of features which would be expected to disrupt the cusp. Baryonic matter and central black holes are factors which contaminate this kind of analysis in other galaxies including our own, but Draco is evidently little more than a spherical clump of self-gravitating dark matter. We can't assume that Draco has a

steep cusp with complete impunity because many things can alter the inner structure of the galaxy, but under a certain set of conditions, such a profile becomes completely reasonable. In the next section, we discuss ways in which a steep cusp might be softened (provided that the relaxation process progressed far enough to form one initially), and why Draco should avoid this softening.

2.3 Retaining a Steep Cusp

Calculated as in eq. (1), R_{min} is only on the order of a few AU ($1 \text{ AU} = 1.5 \times 10^{13} \text{ cm}$) to a few $\times 10^{15} \text{ cm}$, depending primarily on the value of $\langle \sigma v \rangle_{\chi\bar{\chi}}$. It stands to reason that external influences such as the tidal force from the Milky Way should have negligible effect on a central cusp that small; tidal truncation is in fact observationally ruled out below a radius of 1 kpc (Kleyna et al., 2001b). But it is important that we consider any other theoretical motivation for disrupting cusps down to such small scales as R_{min} . (The appropriate scale to verify for the validity of the gamma ray limits derived herein is indeed R_{min} ; however, as described in subsection 3.2, the radio synchrotron emanates from within a larger radial size $\sim 0.01 \text{ pc}$.) Several such ways to spoil the cusp are addressed here.

(1) It has been proposed that the supermassive black holes found at the centers of large galaxies will change the dark halo cusps, although how they will change the cusps is a matter of some debate. One argument is that a cusp would steepen into a spike due to accretion of DM onto the black hole (Gondolo and Silk, 1999; Gondolo, 2000), causing enhanced annihilation signatures. If so, then any value of the cusp slope index γ over-produces the expected synchrotron signature beyond observational limits. Alternatively, if nuclear black holes pair up in a binary system during a galaxy merger, as one would expect after dynamical friction pulls both holes to the center of the remnant but before they merge into one hole, then the two-body interactions of the holes would throw other masses out of the center (Milosavljević et al., 2001; Merritt and Cruz, 2001). In that case, both baryonic and dark matter would be affected, and the central cusp would be softened; this result is corroborated by an HST survey (Ravindranath, Ho, and Filippenko, 2001), in that central mass deficits in galaxies (i.e., the departure from a cusp) correlate with the masses of their central black holes.

The relevance of this issue depends on whether or not the Draco dwarf harbors a central black hole. As a general trend, it appears that ellipticals and spheroidals brighter than approximately $2 \times 10^{10} L_{\odot}$ do have supermassive black holes, and dimmer galaxies may not (Sparke and Gallagher, 2000), although there are exceptions. For Draco, unless its history is devoid of mergers, the observed velocity curve should reveal a softened core if there were a supermassive central hole. In the absence of direct evidence for such a hole in Draco, we assume that Draco has none, so that the concerns of the previous paragraph only afflict other galaxies.

(2) Could the cusp be scattered by baryonic matter? El-Zant, Shlosman, and Hoffman (2001) have proposed that the

missing cusps in galaxy cores are due to interactions between dark matter and clumpy baryons, in a scheme which always transfers energy from baryons to WIMPs, causing the baryonic matter domination at small radii. Interestingly, many dwarf galaxies exhibit rising rotation curves out to scales like ~ 10 kpc (see the discussion of dwarf galaxies in Navarro, Frenk, and White (1996)). But Draco, with a much higher M/L ratio, has constant velocity across all observed radii. So even if baryonic matter is to blame for destroying cusps in other galaxies, it has a diminished role in Draco.

(3) Some nonlinear dynamical process among clumpy dark matter might expand the central region, by way of the halo forming from a swarm of smaller and denser subhalos which formed earlier. For our purposes, the effect is difficult to estimate, because current simulations have not resolved much below Draco mass objects. However, there is no indication of a cutoff immediately below this mass scale in the simulations (Moore et al., 2001). Metcalf (2001) finds that even very small objects ($> 10^3 M_\odot$, should they exist) are dense enough to survive tidal disruption. But these objects are too light to experience significant dynamical friction, so they still behave as collisionless DM, and probably do not disrupt the smooth halo. Objects near the mass of the host halo will settle to the center due to dynamical friction (Metcalf and Madau, 2001), and be tidally stripped when they pass inside the central region (Metcalf, 2001). So is there an intermediate scale dark object which does ruin the $\sim 10^8 M_\odot$ halo's cusp? There is no immediately obvious reason why not.

However, it is interesting to note that globular clusters (typically $\sim 10^6 M_\odot$) are not observed to contain significant amounts of dark matter (a typical globular cluster ratio of $2 M_\odot/L_\odot$ is given by Binney and Tremaine (1987)), which may mean that dark matter clumps of mass scales below those of dwarf galaxies are suppressed for some reason. In fact, it has been proposed that globular clusters could be disrupted remains of larger dwarf galaxies (Côté, West, and Marzke, 2001), because their numbers are appropriate to explain the missing dwarf galaxies expected by CDM theory.

The possibility that intermediate mass dark objects don't exist in large numbers can be dramatically strengthened by upcoming observations. If substructure DM clumps form on small mass scales like $10^6 M_\odot$, then thousands of such clumps will be observable above the cosmic microwave background by their annihilation products (e.g., by the Planck experiment), even if they turn out to obey gently cusped NFW profiles (Blasi, Olinto, and Tyler, 2002). These observations are sensitive to a lower mass cutoff on substructure DM clumps. So if more than ~ 1000 sources are not found, then it is difficult to see how a steep cusp could be inhibited in a dwarf galaxy like Draco by dark matter alone. (This holds unless the WIMPs do not annihilate like neutralinos, but that result is immediately consistent with non-detections from Draco anyway.) If these CMB foreground sources are found, then the results in section 4 of this paper can be construed as either limits on neutralino properties or evidence for important dark substructure dynamics preventing steep cusps in the cores of dwarf galaxies.

3 Annihilation Signals

3.1 Gamma rays

Supposing that Draco has a dark SIS profile populated by annihilating neutralinos, one can calculate the gamma ray emission caused by decaying pions made in the $\chi\bar{\chi}$ annihilation: $\pi^0 \rightarrow \gamma\gamma$. The rate of gamma ray production above a threshold energy E_0 per time per volume is

$$q_\gamma = n_\chi^2 \langle \sigma v \rangle_{\chi\bar{\chi}} N_\gamma(E_\gamma > E_0). \quad (5)$$

In this work, we adopt a method of approximation that has been used previously in this context (Berezinsky, Gurevich, and Zybin, 1992; Bergström, Edsjö, and Ullio, 2001) for the number of gamma rays produced above threshold per annihilation, $N_\gamma(E_\gamma > E_0)$. The π^0 production by $\chi\bar{\chi}$ annihilation follows

$$\frac{dN_\pi}{dx} \simeq K_\pi e^{-8x} / (x^{1.5} + 0.00014), \quad (6)$$

with $x \equiv E_\pi / m_\chi c^2$, and K_π constant. For the two photon decay process, the probability of making a photon per range of energy E_γ is $2/E_\pi$. Then we have

$$N_\gamma(E_\gamma > E_0) = K_\gamma \int_{E_0/m_\chi c^2}^1 \frac{e^{-8x}}{(x^{1.5} + 0.00014)} \frac{dx}{x}, \quad (7)$$

where the constant K_γ is set by requiring that one third of the total energy released per neutralino annihilation go into gamma rays, because about one third of the particles produced by $\chi\bar{\chi}$ are neutral pions, which decay via the two photon channel. The remaining two thirds are divided equally among π^+ and π^- particles, whose decay products will be the topic of the next subsection. Berezinsky, Gurevich, and Zybin (1992) have shown that gamma ray line flux due to $\chi\bar{\chi} \rightarrow \gamma\gamma$ makes a very minor correction to the flux predicted above, and we will ignore it here.

To get the observable gamma ray flux (photons $\text{cm}^{-2} \text{s}^{-1}$), integrate eq. (5) over the volume of the source, and divide by $4\pi d^2$. This procedure is specific to the r -dependence of the halo model used, but for example, with an SIS halo where $n_\chi = Ar^{-2}$,

$$F_\gamma(E_\gamma > E_0) = \frac{4A^2}{3d^2} \langle \sigma v \rangle_{\chi\bar{\chi}} N_\gamma(E_\gamma > E_0) \frac{1}{R_{\min}}, \quad (8)$$

where d is the distance from the Earth. For cusps steeper than $\gamma = 1.5$, the general result is that the gamma ray flux varies as $R_{\min}^{3-2\gamma}$. At $\gamma \geq 1.5$, as in the Moore profile where $\gamma = 1.5$, the integral over the volume of the source becomes dependent on an outer radius instead of R_{\min} . For example, in the Moore profile, the emission region is of size $\sim r_s$ and the flux depends only very weakly on R_{\min} . For an isothermal halo with a constant density core, eq. (8) applies, with R_{\min} replaced by R_{core} . Section 4 gives the results of this process for Draco.

3.2 Radio Synchrotron

The charged pions produced in $\chi\bar{\chi}$ annihilations decay as

$$\pi^+ \rightarrow \mu^+ \nu_\mu \text{ and } \pi^- \rightarrow \mu^- \bar{\nu}_\mu. \quad (9)$$

Muons subsequently decay via

$$\mu^+ \rightarrow e^+ \bar{\nu}_\mu \nu_e \text{ and } \mu^- \rightarrow e^- \nu_\mu \bar{\nu}_e. \quad (10)$$

Electrons and positrons produced in this way will generate synchrotron radiation if there are ambient magnetic fields. This calculation was first done by Berezhinsky, Gurevich, and Zybin (1992) for the Galactic center, and is repeated in Blasi, Olinto, and Tyler (2002) and here, with multiple new corrections applied. (For some parts of this section, cgs units have been provided for clarity.)

We need to know the number spectrum of electrons and positrons produced in each neutralino annihilation, dN_e/dE_e . We use a formulaic simplification of this function (Hill, 1983), which reduces to $dN_e/dE_e \sim E_e^{-3/2}$ at low energy, and drops toward zero as it nears the cutoff $E_e \simeq m_\chi$. The full expression used is

$$\frac{dN_e}{dE_e} = \int_{E_e}^{m_\chi c^2} \int_{E_\mu}^{E_\mu/\bar{r}} W_\pi \frac{dN_\mu^{(\pi)}}{dE_\mu} \frac{dN_e^{(\mu)}}{dE_e} dE_\pi dE_\mu, \quad (11)$$

where $\bar{r} \equiv (m_\mu/m_\pi)^2$,

$$W_\pi = \frac{15}{16} \left(\frac{E_\pi}{m_\chi c^2} \right)^{-3/2} \left(1 - \frac{E_\pi}{m_\chi c^2} \right)^2, \quad (12)$$

and

$$\frac{dN_\mu^{(\pi)}}{dE_\mu} = \frac{1}{E_\pi} \frac{m_\pi^2}{m_\pi^2 - m_\mu^2} \quad (13)$$

and

$$\frac{dN_e^{(\mu)}}{dE_e} = \frac{2}{E_\mu} \left[\frac{5}{6} - \frac{3}{2} \left(\frac{E_e}{E_\mu} \right)^2 + \frac{2}{3} \left(\frac{E_e}{E_\mu} \right)^3 \right]. \quad (14)$$

These last two equations, eqs. (13) and (14), give the decay products from charged pion and muon decays, respectively. Note that dN_e/dE_e without any superscripting indicates the number spectrum of electrons from the entire chain of decays following a single $\chi\bar{\chi}$ annihilation.

The charged particle injection is

$$q_e = n_\chi^2 \langle \sigma v \rangle_{\chi\bar{\chi}} \left(\frac{dN_e}{dE_e} \right), \quad (15)$$

so that $q_e \sim E_e^{-3/2} r^{-2\gamma}$ because $n_\chi \sim r^{-\gamma}$ for a cusp with logarithmic slope $-\gamma$. Throughout this subsection we will continue to use this generic cusp. The electron distribution is

$$\frac{dn_e}{dE_e} = q_e \tau, \quad (16)$$

where $\tau = \tau(E_e, r)$ is the average lifetime of an electron of energy E_e . There are four processes limiting the life of an

electron considered in this work, and for any given combination of E_e and r , the lifetime is the fastest of these processes. They are: (1) loss of energy by synchrotron radiation, (2) loss of energy by inverse Compton scattering (ICS) against the cosmic microwave background (CMB), (3) loss of energy by ICS against the local synchrotron photons, and (4) annihilation with positrons. For pair annihilation, there is a characteristic time scale; for the other processes, there is a loss rate dE_e/dt for which

$$\tau \simeq \frac{E_e}{dE_e/dt}. \quad (17)$$

At a given E_e , we find that e^+e^- pair annihilation can be dominant in the center of the clump, followed outward by a shell dominated by ICS against synchrotron photons, followed by the outermost shell dominated by synchrotron losses and ICS against the CMB. The region dominated by ICS against synchrotron photons generates most of the total flux from the clump. Synchrotron ICS and e^\pm pair annihilation are discussed below; both have the effect of removing emitters preferentially from the dense central regions, reducing the synchrotron signal.

Employing a formula from Rybicki and Lightman (1979), the synchrotron power is

$$\frac{dE_{\text{syn}}}{dt} = 1.6 \times 10^{-15} B_\mu^2 E_e^2 \text{ erg/s}, \quad (18)$$

for $B_\mu = |\vec{B}|$ in microgauss. It is convenient to approximate the synchrotron as if all the radiation were emitted at the peak frequency (which is different for each electron):

$$\nu_{\text{peak}} = 1.5 \times 10^{12} B_\mu E_e^2 \text{ Hz}. \quad (19)$$

Eqs. (15), (18), and (19) combine to give the radio signal we seek as follows:

$$j_\nu = \frac{dn_e}{dE_e} \frac{dE_e}{d\nu} \frac{dE_{\text{syn}}}{dt} \frac{\text{erg}}{\text{cm}^3 \text{ s Hz}}. \quad (20)$$

The luminosity is the integral of j_ν over the volume of the DM source.

At this point, some details need to be considered. The above picture is correct but not complete; three amendments are analyzed presently.

(1) *Inverse Compton scattering* of relativistic electrons and positrons against the synchrotron photons created in the DM clump is the most important correction. ICS power is (Rybicki and Lightman, 1979)

$$\frac{dE_{\text{ics}}}{dt} = \frac{4}{3} \sigma_T c \beta^2 \gamma^2 U_{\text{ph}}, \quad (21)$$

where $\sigma_T = 6.65 \times 10^{-25} \text{ cm}^2$ is the Thomson cross section appropriate in the limit $h\nu \ll m_e c^2$, $\beta \simeq 1$, and U_{ph} is the energy density in the photon field. Therefore, the photon population with the greatest energy density controls the rate of ICS. For the CMB,

$$U_{\text{cmb}} = aT_{\text{cmb}}^4, \quad (22)$$

for $a = 7.56 \times 10^{-15} \text{ erg cm}^{-3} \text{ K}^{-4}$ and $T_{\text{cmb}} = 2.728 \text{ K}$; whereas for the synchrotron photon population, one must integrate j_ν over all possible e^\pm energies (from $m_e c^2$ to $m_\chi c^2$) and over all lines of sight.

Unfortunately, this double integration for U_{syn} requires *a priori* knowledge of the electron distribution in energy (E_e) and in space (r), since dn_e/dE_e is contained in j_ν via eq. (20). The electron distribution depends on the rate of ICS losses and depends therefore, in turn, on U_{syn} (via eqs. (16), (17), and (21)). Consequently, our full calculation of dn_e/dE_e is numerical and iterative; however, some assumptions and simplifications will get us the broad brush answer as well.

First, assume that the solution takes the form of separable power laws which we will solve for:

$$\frac{dn_e}{dE_e}(E_e, r) \sim E_e^\alpha r^\beta. \quad (23)$$

Then we need a further assumption, that the dominant contribution to the photon density at some point r comes from the region inside r only. One might expect this to hold, since all photons generated inside r will pass through r , but only a small fraction of those produced outside r will. This is still an unjustified assumption which can be checked afterward by trying alternative values for the exponent β ; the numerical results do validate the assumption as well.

Let's define a shell of width Δr such that a photon spends $\Delta r/c$ time in that region. Given these assumptions, and using r' as a radial variable of integration,

$$\frac{dU_{\text{syn}}}{dE_e} \sim \frac{1}{4\pi r^2 \Delta r} \int_{R_{\text{min}}}^r E_e^\alpha r'^\beta \frac{dE_{\text{syn}}}{dt} \frac{\Delta r}{c} 4\pi r'^2 dr'. \quad (24)$$

(The region inside R_{min} makes its own contribution as well, but it turns out to be small.) Combining with eq. (18), we get $dU_{\text{syn}}/dE_e \sim E_e^{\alpha+2} r^{\beta+1}$. Then upon integrating over E_e , we get $U_{\text{syn}} \sim r^{\beta+1}$.

From eq. (17),

$$\tau \sim E_e^{-1} r^{-\beta-1}, \quad (25)$$

and from eqs. (15) and (16),

$$\frac{dn_e}{dE_e} \sim (E_e^{-3/2} r^{-2\gamma})(E_e^{-1} r^{-\beta-1}). \quad (26)$$

So, simply equating the exponents in eqs. (23) and (26), we obtain $\alpha = -5/2$ and $\beta = -\gamma - 1/2$, or

$$\frac{dn_e}{dE_e} \sim E_e^{-5/2} r^{-\gamma-1/2}. \quad (27)$$

This holds wherever electron losses are fastest by ICS in the synchrotron photon field. In the case of losses being dominated by synchrotron radiation and ICS against the CMB instead, the loss mechanism is independent of r , so we would have $dn_e/dE_e \sim E_e^{-5/2} r^{-2\gamma}$. Since the two forms of electron losses have different power laws in r (and the same power law in E_e), there is a transition radius $R_{\text{ics, syn}}$ (which is independent of E_e) between the two behaviors.

For Draco, $R_{\text{ics, syn}} \simeq 0.01 \text{ pc}$, depending loosely on the WIMP mass and the ambient magnetic field strength. Inside this radius, the electron population is limited by ICS against synchrotron photons and decreases as $r^{-\gamma-1/2}$; outside this radius the electron population is limited by synchrotron losses and ICS against the CMB, and decreases as $r^{-2\gamma}$. Interestingly, $R_{\text{ics, syn}}$ becomes the characteristic observable size of the radio source, and it is resolvable to interferometers with baselines of order 100 km.

(2) *Pair annihilation* between e^- and e^+ particles would have an important role in determining the flux from a DM source in the absence of the ICS described above. But in the presence of ICS losses, pair annihilation makes little difference to the resulting radio flux.

The pair annihilation process is still important, because it reduces the population of the lower energy pairs, which would otherwise upscatter photons frequently enough to spoil the synchrotron spectrum. Although in much of the DM source, most electrons Compton scatter with photons, most photons do not Compton scatter with electrons because they escape first; it is these synchrotron photons whose survival we are considering now. In the case of Draco, and for the most optically thick line of sight through its diameter, the optical depth for a photon against synchrotron self Compton scattering is of order 10^{-3} , making it a negligible effect on the resulting observable spectrum. But one needs to calculate the pair annihilation rate to discover that fact.

We can estimate the e^\pm lifetime for the case where electrons annihilate before they lose a significant fraction of their original energy via synchrotron or ICS as

$$\tau_{e^\pm} \simeq \frac{1}{\langle n_{e^-} \sigma_{e^\pm} v_{e^-} \rangle} \quad (28)$$

with $v_e \simeq c$, and the angle brackets indicating an average over E_{e^-} . (This is equally valid if we interchange all the plus and minus signs, but we will keep track of signs in order to distinguish between particles and antiparticles, for clarity.)

With eq. (16), we have

$$\frac{dn_{e^+}}{dE_{e^+}} = \frac{q_{e^+}}{\langle n_{e^-} \sigma_{e^\pm} v_{e^-} \rangle}. \quad (29)$$

The term in angle brackets is computed from the equations in Svensson (1982) (also consistent with Coppi and Blandford (1990)), particularly

$$\langle \sigma v \rangle_{e^\pm} = \int_1^\infty f(\gamma_+) \int_1^\infty f(\gamma_-) (\overline{\sigma v})_{e^\pm} d\gamma_- d\gamma_+, \quad (30)$$

where f is a distribution function for e^\pm of Lorentz factor γ_\pm , and $(\overline{\sigma v})_{e^\pm}$ is the angle averaged reaction rate per pair given explicitly in Svensson (1982); here we quote the asymptotic form, although the full formula has been used in the numerical work described in this paper:

$$(\overline{\sigma v})_{e^\pm} \simeq \frac{\pi e^2}{m_e c} \frac{1}{\gamma_+ \gamma_-} (\ln 4\gamma_+ \gamma_- - 2) \quad (\gamma_+, \gamma_- \gg 1). \quad (31)$$

Eq. (30) is adapted by replacing $f(\gamma_-) \rightarrow dn_e/dE_e$, and $f(\gamma_+) \rightarrow \delta(\gamma_+)$; that is, for a *chosen* positron of energy γ_+ , its survival time is a function of the electron distribution.

Then, we have $\langle n_{e^-} \sigma_{e^\pm} v_{e^-} \rangle$ expressed as an energy integral which depends on the e^\pm distribution that we're trying to solve for. Therefore this pair annihilation calculation must be done numerically. The dependences here are nested infinitely, which is to say that τ_{e^+} depends on n_{e^-} which depends on τ_{e^-} which depends on n_{e^+} and so on. It is most efficient to try to determine the correct dependences *a priori*, and then integrate accordingly.

So if we neglect the natural logarithm factor built into $(\overline{\sigma v})_{e^\pm}$ from eq. (31), because it evolves slowly compared with powers of γ_+ and γ_- , then we can proceed to find the energy dependence for τ_{e^+} to within a factor of about $E_{e^+}^{\pm 0.05}$ in accuracy.

The reaction rate for a given positron is $\langle n_{e^-} \sigma_{e^\pm} v_{e^-} \rangle$, which varies inversely with electron energy (any other hypothesis leads to a contradiction). Therefore, the positron will preferentially annihilate against an electron at the low end of the energy distribution, so that in eq. (29), $\langle \sigma_{e^\pm} v_{e^-} \rangle \sim E_{e^+}^{-1}$, and n_{e^-} is roughly constant. That is, a given positron of any energy sees essentially the same distribution of target electrons, so to a first approximation, it is sufficient to replace the electron distribution with a single population at energy $E_{e^-} \simeq m_e c^2$. By that rationale, $\tau_{e^+} \sim E_{e^+}$.

With this last result in hand, it becomes useful to use

$$\tau_{e^-} \simeq \tau_{e^+} \left(\frac{E_{e^-}}{E_{e^+}} \right) \quad (32)$$

when doing the full numerical integral over target electron energies, to avoid the infinite nesting problem. At low energies where $dN_e/dE_e \sim E_e^{-3/2}$, this means that $dn_e/dE_e \sim E_e^{-1/2}$ and $n_e \sim E_e^{1/2}$ (where the subscript e refers to either an electron or a positron).

The distribution in space, rather than energy, is easier to determine. In order to satisfy eq. (29) with the injection $q_e \sim r^{-2\gamma}$ set by a cuspy DM profile, we must have $dn_e/dE_e \sim r^{-\gamma}$. (As before, $-\gamma$ is the halo profile logarithmic slope, while γ_+ and γ_- are Lorentz factors.) Then for a region whose e^\pm losses are fastest by pair annihilation, we have

$$\frac{dn_e}{dE_e} \sim E_e^{-1/2} r^{-\gamma}. \quad (33)$$

So now we have another transition radius between the $r^{-\gamma}$ pair annihilation distribution and the $r^{-\gamma-1/2}$ ICS distribution, which we designate $R_{\text{ann,ics}}$. If $R_{\text{ann,ics}} > R_{\text{min}}$, then we add a pair annihilation dominated central region to the picture described above regarding ICS. But for most choices of m_χ and Draco's magnetic field strength, $R_{\text{ann,ics}} < R_{\text{min}}$ for electrons radiating at frequencies of interest, and the distribution flattens at the center before the density can get high enough to create a pair annihilation dominated region.

(3) *Synchrotron self absorption (SSA)* is where an electron in a magnetic field can absorb the synchrotron photon's energy. Still linking photon frequency to the energy of its emitting electron with eq. (19) for simplicity, the appropriate adaptation from Rybicki and Lightman (1979) yields the

per-unit-length absorption coefficient:

$$\alpha_\nu = -\frac{c^2}{8\pi\nu} \frac{dE_{\text{syn}}}{dt} \left[\frac{\partial}{\partial\nu} \left(\frac{1}{\nu} \frac{dn_e}{d\nu} \right) \right]. \quad (34)$$

SSA absorbers of a particular photon are electrons of similar energy to the original synchrotron emitter which made the photon. As such, SSA is only effective below some ν_{crit} , where the corresponding electrons are more numerous.

The source function for an absorbing source is $S_\nu = j_\nu/\alpha_\nu$, and the optical depth is

$$\tau_\nu = \int \alpha_\nu dz, \quad (35)$$

where z is a line-of-sight coordinate. The flux density from such a source at distance d from the Earth is obtained by summing over each line of sight through the DM clump:

$$I_\nu = \frac{1}{4\pi d^2} \int_0^{R_{\text{cl}}} 2\pi b S_\nu (1 - e^{-\tau_\nu}) db \frac{\text{erg}}{\text{cm}^2 \text{ s Hz}}. \quad (36)$$

The SSA cutoff frequency ν_{crit} depends in part on the absorber density, and without ICS or e^\pm pair annihilation effects, SSA would be the most important correction to the calculated flux in a steep cusp. SSA has been included in the calculations performed here, but since the central absorber population is diminished by ICS, it is of small importance. Using appropriate parameters for Draco, we find $\nu_{\text{crit}} \simeq 10$ MHz, whereas the limiting observations discussed in the next section are at 4.9 GHz. (It is fortunate that SSA has little impact on the problem, because otherwise it would create serious complications in the calculation of ICS against the synchrotron photon field.)

4 Results

Supersymmetric dark matter has a number of variable parameters which affect its annihilation and clustering properties. However, these parameters boil down to only two relevant quantities for annihilation signature searches, and those are m_χ and $\langle \sigma v \rangle_{\chi\bar{\chi}}$. Given external constraints on a dark matter source (such as Draco's total mass and the matter density local to it, in the present case), the mass m_χ determines the χ number density. The more massive the particle, the fewer are needed, so the annihilations are less frequent. We present here the collection of m_χ and $\langle \sigma v \rangle_{\chi\bar{\chi}}$ values available to the neutralino, derived from observations of Draco.

Before proceeding to these limits, we note for comparison another indirect detection approach considered in the literature, that of detecting neutrinos (as from eqs. (9) and (10)) coming from neutralino annihilations at the center of the Earth and the Sun. By elastic scattering with nuclei in the Sun or Earth, a WIMP can lose enough energy to be gravitationally captured by that body. This captured population is the source of the neutrino signal in question. Supersymmetric parameter space can be ruled out in this way by neutrino telescopes such as Baksan or AMANDA (for example, see Bergström, Edsjö, and Gondolo (1997) and Ahrens et al.

(2002)). This method can currently eliminate more parameter space than direct detection experiments, and less than the Draco EGRET limits as calculated herein. The constraints from Draco require the extrapolation of its halo density profile to small radii; the constraints from neutrino telescopes instead require the additional steps associated with elastic scattering, capture, and neutrino propagation through matter. Of course, this approach and the one used in the present work are both indirect detection scenarios; for a review of direct experimental searches, see e.g. Morales (2001).

4.1 Gamma Ray Constraints

Gamma ray data specifically on Draco are lacking, so the current limiting observations come from an all-sky survey. The EGRET (Energetic Gamma Ray Experiment Telescope) instrument, flying on the CGRO satellite (Compton Gamma Ray Observatory), is a pair production telescope (see Mattox et al. (1996) for an introduction to EGRET and its data analysis). As such, its useful beam width is around 30° , making it well suited for a full sky survey; its energy range is ~ 30 MeV to below ~ 100 GeV (Sreekumar et al., 1998).

EGRET sources are usually counted by their photons above 100 MeV; however, Lamb and Macomb (1997) have performed a separate binning of the data, making a catalog of gamma ray sources above 1 GeV, which is of particular interest here. The least significant detection (4σ) in the catalog, with the least flux, is the Large Magellanic Cloud (LMC), at $(1.1 \pm 0.4) \times 10^{-8}$ photons $\text{cm}^{-2} \text{s}^{-1}$ above 1 GeV. We therefore take 10^{-8} photons $\text{cm}^{-2} \text{s}^{-1}$ as the flux limit for detection, and require that Draco emit less.

In fact, since this limit is only based on non-inclusion in the GeV catalog, specific knowledge of the exposure on Draco could result in a bound somewhat better than the one derived herein. A subsequent analysis of the EGRET data provides an estimate of the instrument's extragalactic gamma ray background (Sreekumar et al., 1998). With Draco located well outside the Galactic disk ($l = 86.37^\circ$, $b = 34.71^\circ$ (van den Bergh, 2000)), this extragalactic component is the primary background source. The extragalactic flux, adapted to the GeV catalog's 30 arcmin pixel size,

$$F_\gamma(E_\gamma > E_0) = 8.6 \times 10^{-11} \left(\frac{E_0}{\text{GeV}} \right)^{-1.1} \frac{\text{photons}}{\text{cm}^2 \text{s}} \quad (37)$$

is well below the level of one photon per minimum EGRET exposure. We therefore separately consider this background in our calculations, conservatively assuming that EGRET's exposure on Draco is their minimum exposure (roughly true), for the case of no photons detected within 30 arcmin. We present this as an example of the type of improvement possible without collecting new data.

In figure 1, we plot the neutralino parameter space. In this figure, we have presented limits derived by use of the SIS halo profile with different curves giving different present and future observational bounds; a comparison of halo models will follow in subsection 4.3. Both EGRET constraints

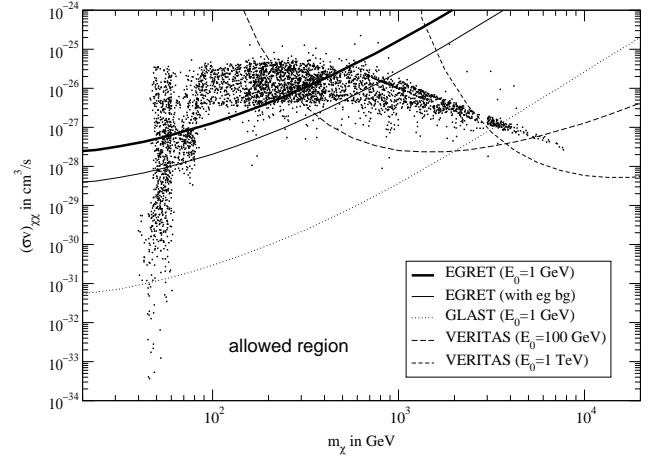


Fig. 1. The $m_\chi - \langle \sigma v \rangle_{\chi\bar{\chi}}$ plane for neutralino dark matter. Curves indicate results where the SIS halo profile has been used. Shown as solid lines are the gamma ray constraints from non-inclusion in the EGRET all-sky survey, where the thick line is the current bound and the thin line is a potential improvement using an estimate of the extragalactic gamma ray background (see text). Both employ a threshold $E_0 = 1$ GeV. Also shown are two dashed lines showing upcoming VERITAS constraints with cutoffs at 100 GeV and 1 TeV, and a dotted line for GLAST at $E_0 = 1$ GeV (sensitivities for all of these taken from Weekes et al. (2001)). The region below the curves is allowed by gamma ray observations. Uncertainties in Draco's mass and distance lead to at most a factor of 3 change in the vertical axis position of these curves. The dots denote typical supersymmetric dark matter properties (Gondolo et al., 2000).

are shown: the current bound (thick solid line), and the example bound with the newer extragalactic background (thin solid line). Points above the curves are prohibited by these observational constraints from Draco.

Two notes should be made regarding accuracy. First, the curves in the figure assume that $M_{\text{Draco}} = 8.6 \times 10^7 M_\odot$, which is measured using observations of its luminous matter (Kleyna et al., 2001a). So this mass samples the inner halo, and the total mass could be higher. In this sense, the curves plotted should be considered conservative. Second, recall from the discussion of R_{min} in subsection 2.1 that a higher estimate of R_{min} would result from a slower relaxation process. At most, this would make these curves less constraining (i.e., raise them) by a factor of about 5.

The dots in the figure survey the possible combinations of m_χ and $\langle \sigma v \rangle_{\chi\bar{\chi}}$ for neutralino dark matter (Gondolo et al., 2000). The dotted region is characteristic of supersymmetric parameters often considered in the literature (e.g., Gondolo and Silk (1999); Baltz et al. (1999)). They are constrained by the requirement that the relic density be cosmologically interesting; that is, large enough to account for a significant component of the matter density without exceeding it. The choice of these “interesting” values is somewhat arbitrary and authors differ slightly, but a restriction like $0.05 \leq \Omega_\chi h^2 \leq 0.5$ as depicted in the figure is typical. It should be noted that values of $m_\chi < 38$ GeV are disfavored by accelerator experiments (Serin, 2000).

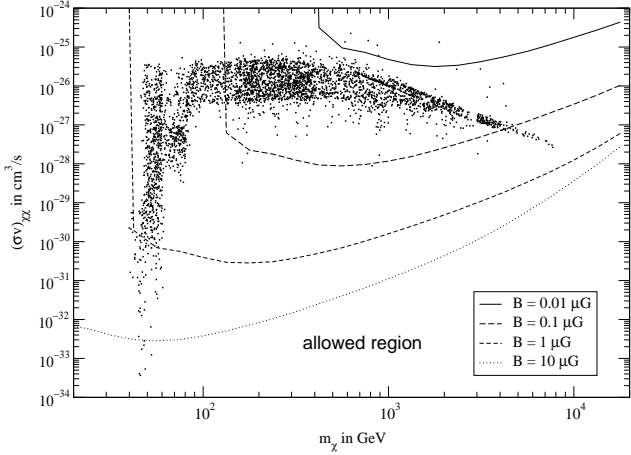


Fig. 2. The $m_\chi - \langle\sigma v\rangle_{\chi\bar{\chi}}$ plane for neutralino dark matter. Curves indicate results where the SIS halo profile has been used. Shown as thin lines are the radio synchrotron constraints from VLA observations. From top to bottom, these lines correspond to magnetic fields of 0.01, 0.1, 1.0, and 10.0 μG in the core of Draco. The region below these curves is allowed by radio observations. Uncertainties in Draco’s mass and distance lead to at most a factor of 3 change in the vertical axis position of these curves. The dots denote typical supersymmetric dark matter properties.

Future gamma ray telescopes offer better constraints. The upcoming satellite mission GLAST (Gamma ray Large Area Space Telescope), will offer much improved constraints as shown in the figure (Gehrels and Michelson, 1999). It is expected to launch in 2005 for a two year all-sky survey, effective between 20 MeV and 300 GeV, with a sensitivity about 20 times better than EGRET at 1 GeV. As can be seen in the figure, GLAST has the potential to rule out most of the neutralino DM parameter space.

Apart from satellite missions, atmospheric Cherenkov telescopes (ACTs) are ideal for measuring at high energy. Rather than detecting the photons via interactions inside the telescope, ACTs count gamma rays by the air showers they produce in the Earth’s atmosphere. Specifically, they respond to Cherenkov light produced by charged particles in the shower traveling faster than the speed of light in air. The next generation gamma ray telescope VERITAS (Weekes et al., 2001) can provide significant benefits for this study with a typical exposure on Draco (we quote here an exposure of 50 hours). Curves for VERITAS with threshold energies of 100 GeV (long dashes) and 1 TeV (short dashes) are depicted in the figure. VERITAS is sensitive between about 50 GeV and 50 TeV; it is expected to see first light in 2002 and become fully operational in 2005.

4.2 Radio Constraints

The applicable radio continuum limits for Draco were performed by Fomalont and Geldzahler (1979), using the VLA (Very Large Array) facility in New Mexico. At 4.9 GHz, they report no flux from Draco above 2 mJy, at the 3σ level. Their search spanned a radius of 4 arcmin around the galaxy center.

Two additional assumptions beyond those discussed in section 2 are needed in order to place a radio limit, because synchrotron emission requires magnetic fields.

First, we must assume a magnetic field strength $|\vec{B}|$ for the core of Draco. No such estimates exist in the literature, so this paper must be viewed as constraining either the neutralino or Draco’s magnetic properties. To give some bearing on the estimation of $|\vec{B}|$, we can consider measurements for other dwarf galaxies. The Magellanic Clouds, for example, each carry fields of $\sim 5 \mu\text{G}$ (Pohl, 1993). A survey of low surface brightness dwarf galaxies (similar to Draco) leads Klein et al. (1992) to infer typical field strengths between 2 and 4 μG , although this survey was conducted near 5 GHz and Draco specifically gives no measured signal there. The dwarf irregular NGC 4449 was found to harbor $\sim 14 \mu\text{G}$ fields despite the lack of ordered rotation (Chyży et al., 2000), suggesting that some non-dynamo process may be sufficient to generate microgauss fields. Based on these data, it seems appropriate to expect $\sim 0.1 - 1 \mu\text{G}$ in Draco, although at present there is no compelling evidence.

Second, not only must there exist magnetic fields, but they also must be sufficiently constricted, so as to trap electrons and positrons long enough for them to radiate. Implicit in the computation of flux from DM sources in this paper is the assumption that e^\pm particles never stray far from their birth places – an assumption of strong magnetic confinement. To begin contemplating this, consider that the gyroradius of any electron relevant to this problem is significantly smaller than the smallest length scale applicable; that is, $R_{\text{gyro}} \ll R_{\text{min}}$. So if we assume that electrons are reflected back and forth along a field line every $10 - 100 R_{\text{gyro}}$, then strong confinement is justified. Klein et al. (1991) notes that magnetic fields do in fact appear to be highly disordered in some dwarf galaxies (Draco not considered), based on lack of radio polarization observed. The confinement time needs to be longer than the inverse Compton time scale against the synchrotron photon field in order to validate our model. This duration is typically around $10^7 - 10^8$ years for key emitting regions in Draco’s halo, depending on neutralino parameters, for 4.9 GHz radiation as limited by the VLA.

These caveats noted, the synchrotron constraints are plotted in figure 2, where again the points above each curve can be ruled out by it. Limits for 0.01, 0.1, 1, and 10 μG fields are shown here for the SIS halo; this choice will be varied in section 4.3. As with figure 1, the possibility that M_{Draco} was underestimated makes these curves conservative.

Although the radio limits are less direct because of assumptions that must be made about the \vec{B} field, they can be stronger than current gamma ray limits. For example, if the field is found to be at least 1 μG and adequately confining, then $\langle\sigma v\rangle_{\chi\bar{\chi}}$ for a 100 GeV neutralino is restricted to be below $\sim 4 \times 10^{-31} \text{ cm}^3/\text{s}$, as compared with $\sim 10^{-28} \text{ cm}^3/\text{s}$ in gamma rays. Heavier neutralinos are strongly constrained at 0.1 μG , but they aren’t limited at all by current gamma measurements. On the other hand, if the magnetic fields are weak, then synchrotron offers no constraint on light χ particles. For example, a 100 GeV neutralino’s annihilation prod-

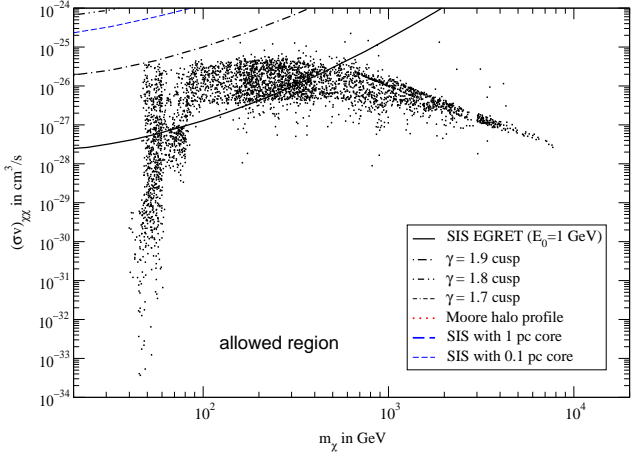


Fig. 3. Parameter space constraints from the EGRET 1 GeV catalog with seven different halo models for Draco. The halos are: cusps with $\gamma = 2.0$ (solid line), 1.9 (dot-dash), 1.8 (dot-dot-dash), and 1.7 (dash-dot), Moore (dotted line), SIS with constant density core at 1 pc (thick dashed line), and SIS with constant density core at 0.1 pc (thin dashed line). The thickest solid line is repeated from the current EGRET bound given in figure 1. Lines not shown indicate that the corresponding halo yields no constraints on this plot.

ucts aren't energetic enough to radiate at 4.9 GHz (where the VLA limit is) if the field is $\sim 0.1 \mu\text{G}$ or below.

As in figure 1, the dots indicate the SUSY parameter space. Here we see the importance of the magnetic field. At $1 \mu\text{G}$ one can exclude the majority of neutralino dark matter candidates; at $0.01 \mu\text{G}$ one can exclude almost none of it.

One further point worth noting is that the gamma ray and radio analyses, taken together, permit us to constrain the magnetic field properties of Draco. If a future gamma ray detection is made, then the corresponding line in the $m_\chi - \langle\sigma v\rangle_{\chi\bar{\chi}}$ plane can be transposed to figure 2, with the result that some values of $|\vec{B}|$ will not be allowed.

4.3 Other Halo Profiles

Figures 1 and 2 solely employ the SIS to generate the limiting curves. In this subsection, we consider the sensitivity of our results to the choice of halo profile.

In figure 3, we present modified gamma ray results corresponding to the current EGRET bound shown as the thick line in figure 1. All curves on this plot correspond to the same EGRET observations above the $E_0 = 1 \text{ GeV}$ threshold, but for different halo models. Figure 4 presents the same halos, but for the GLAST curve from figure 1 with $E_0 = 1 \text{ GeV}$.

The halo models considered all assume spherical symmetry. They are: cusped profiles with $\gamma = 2.0$ (SIS), 1.9, 1.8, and 1.7, the Moore profile as described in subsection 2.1, and the SIS truncated with constant density cores of radius 1 pc and 0.1 pc (the velocity dispersion data extend down to $\sim 10 \text{ pc}$). Figures which omit some of these curves do so because those curves do not constrain any of the parameter space shown. For example, with Draco modeled by the Moore profile, the EGRET data are insufficient to constrain

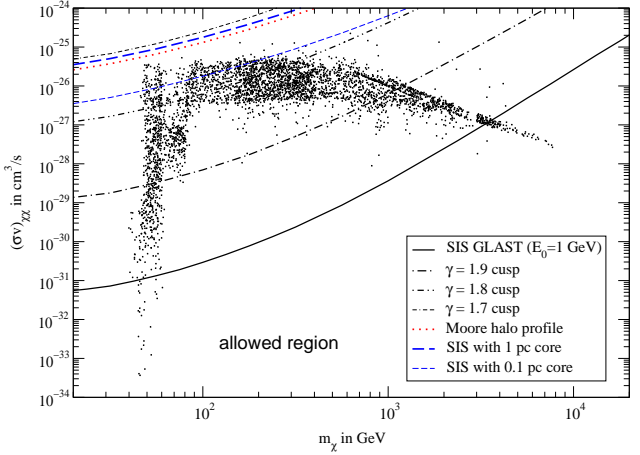


Fig. 4. Same as figure 3, but now showing modifications to the GLAST line from figure 1, rather than EGRET.

$\langle\sigma v\rangle_{\chi\bar{\chi}}$ below $\sim 10^{-24} \text{ cm}^3/\text{s}$; one can do somewhat better in the future with GLAST (figure 4).

For the radio case, the corresponding results are presented in figure 5 for $|\vec{B}| = 0.1 \mu\text{G}$, and in figure 6 for $|\vec{B}| = 1 \mu\text{G}$. In each figure, the same seven halo models are shown as in figures 3 and 4, including the appropriate SIS curve from figure 2.

The cusps $\gamma = 2.0, 1.9, 1.8,$ and 1.7 are calculated with the full inverse Compton scattering corrections described in subsection 3.2. Applying eq. (27) yields dn_e/dE_e dependences which go as $r^{-2.5}, r^{-2.4}, r^{-2.3},$ and $r^{-2.2}$, respectively.

Inverse Compton scattering does not play a significant role in the SIS core cases or in the Moore case, because in each of these halos, the primary emitting region is outside of $R_{\text{ics, syn}}$. The Moore case turns out to create a diffuse enough collection of electrons and positrons that synchrotron self absorption is also negligible, although SSA does significantly affect the results for the isothermal core models.

It is interesting to note that for both gamma ray and radio constraints, the Moore profile yields more flux than a $\gamma = 1.7$ cusp, even though the inner Moore halo only has $\gamma = 1.5$. This is a result of the fact that the Moore profile does not extend as $r^{-1.5}$ indefinitely, but rather is concentrated into r_s . This concentration effect makes up for the lower γ exponent.

From figures 3 through 6, it is clear that the choice of halo model is of great importance in determining the resulting dark matter constraints. Even $\rho \sim r^{-1.9}$ yields weak limits with EGRET data. With GLAST, many of the steeper models are valuable, but less dense ones are not. In the radio, a magnetic field of $0.1 \mu\text{G}$ is roughly as constraining at high m_χ values as GLAST is at lower m_χ values. At $1 \mu\text{G}$, the situation is much better, with all examined profiles generating strong constraints. In this case, the Moore halo too constrains WIMPs well, although the Moore profile is not particularly constraining in any of the other cases considered. The primary lesson from these example cases is that the results do vary appreciably even among relatively steep

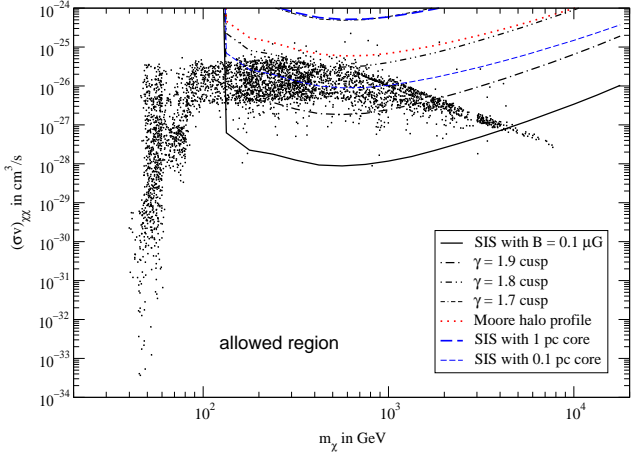


Fig. 5. Parameter space constraints from the VLA with seven different halo models for Draco, assuming a magnetic field strength $|\vec{B}| = 0.1 \mu\text{G}$. The halo modifications are the same as those in figures 3 and 4.

cusps, underscoring the importance of pinning down Draco’s central density structure accurately.

5 Summary

This paper applies gamma ray and radio observational limits to the behavior of dark matter in the Draco dwarf galaxy, only 79 kpc distant from the Earth. Recent measurements of stellar velocities in Draco suggest that it is extremely dark matter dominated, and that its halo distribution is nearly isothermal. Because such a halo should be densely concentrated at the center, we expect WIMP annihilation to proceed rapidly there, producing observable gamma ray and synchrotron radiation.

Current limits derived herein impose restrictions on the nature of the dark matter particle. If it is a neutralino (or simply annihilates into pions like one) then figures 1 through 6 constrain the mass and annihilation cross section available to it. These results emphasize the importance of the choice of halo model for Draco. Our strongest constraints emerge with the SIS profile. In this case, EGRET data restrict much of the supersymmetric parameter space, and if Draco has a suitable magnetic field, then the VLA data can exclude significantly more of it. Other halo profiles with a core or a less steep cusp generally become significantly constraining with future gamma ray experiments, or in the radio with magnetic fields in the μG range.

An important conclusion from this work is that further particle dark matter research would be well served by increasingly detailed studies of Draco.

Acknowledgements. Thanks to Angela Olinto, Josh Frieman, Rich Kron, and Jim Truran for evaluating the topic, suggesting avenues to consider, and examining the manuscript. I also thank Pasquale Blasi for introducing me to this line of research, Paolo Gondolo for providing SUSY model points, and Argyro Tasitsiomi for many useful

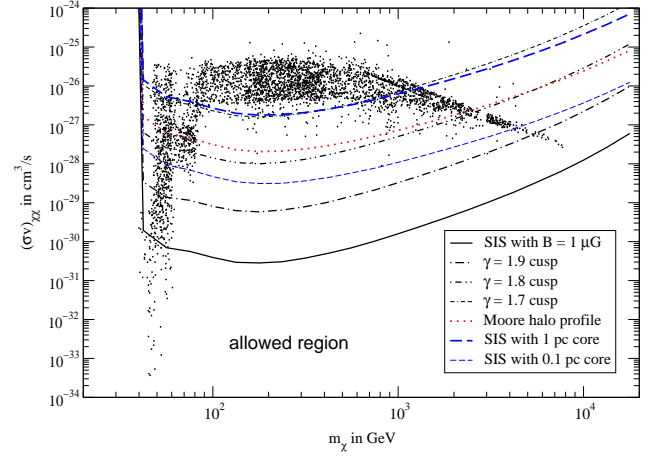


Fig. 6. Same as figure 5, but now showing modifications to the $|\vec{B}| = 1 \mu\text{G}$ line from figure 2.

and relevant conversations. This work was supported by the NSF through grant AST-0071235 and DOE grant DE-FG0291 ER40606.

References

- Ahrens, J. et al. (AMANDA collaboration), astro-ph/0202370.
- Baltz, E.A., Briot, C., Salati, P., Taillet, R., and Silk, J., Phys. Rev. D 61, 023514, 1999.
- Berezinsky, V., Gurevich, A.V., and Zybin, K.P., Phys. Lett. B 294, 221, 1992.
- Berezinsky, V., Bottino, A., and Mignola, G. Phys. Lett. B 325, 136, 1994.
- Bergström, L., Edsjö, J., Gondolo, P., Ullio, P., Phys. Rev. D 59, 043506, 1999.
- Bergström, L., Edsjö, J., and Gondolo, P., Phys. Rev. D 55, 1765, 1997.
- Bergström, L., Edsjö, J., and Ullio, P., Phys. Rev. Lett. 87, 251301, 2001.
- Binney, J. and Tremaine, S., “Galactic Dynamics”, Princeton, NJ: Princeton University Press, 1987.
- Blasi, P., Olinto, A.V., and Tyler, C., astro-ph/0202049.
- Calcáneo-Roldán, C. and Moore, B., Phys. Rev. D 62, 123005, 2000.
- Chyży, K.T., Beck, R., Kohle, S., Klein, U., Urbanik, M., Astron. Astrophys. 355, 128, 2000.
- Coppi, P.S. and Blandford, R.D., MNRAS 245, 453, 1990.
- Côté, P., West, M.J., and Marzke, R.O., Ap. J. 567, 853, 2002.
- Crane, P. et al., Astron. J. 106, 1371, 1993.
- de Blok, W.J.G., McGaugh, S.S., and Rubin, V.C., Astron. J., 122, 2396, 2001.
- El-Zant, A., Shlosman, I., and Hoffman, Y., Ap. J. 560, 636, 2001; ibid. astro-ph/0108327.
- Fomalont, E.B., and Geldzahler, B.J., Astron. J., 84, 12, 1979.
- Gebhardt, K. et al., Astron. J. 112, 105, 1996.
- Gehrels, N. and Michelson, P., Astropart. Phys. 11, 277, 1999.
- Ghigna, S., Moore, B., Governato, F., Lake, G., Quinn, T., Stadel, J., MNRAS 300, 146, 1998.
- Gondolo, P., Nucl. Phys. Proc. Suppl. 35, 148, 1994.
- Gondolo, P., Phys. Lett. B 494, 181, 2000.
- Gondolo, P., Edsjö, J., Bergström, L., Ullio, P.,

and Baltz, E.A., astro-ph/0012234. Also see <http://www.physto.se/~edsjo/darksusy>.

Gondolo, P. and Silk, J., Phys. Rev. Lett. 83, 1719, 1999.

Hill, C.T., Nucl. Phys. B224, 469, 1983.

Jungman, G., Kamionkowski, M., and Griest, K., Phys. Rep. 267, 195, 1996.

Klein, U., Proc. ASA 9 (2), 253, 1991.

Klein, U., Giovanardi, C., Altschuler, D.R., Wunderlich, E., Astron. Astrophys. 255, 49, 1992.

Klenya, J., Wilkinson, M.I., Evans, N.W., Gilmore, G., MNRAS 330, 792, 2002.

Klenya, J., Wilkinson, M.I., Evans, N.W., Gilmore, G., Ap. J. 563, L115, 2001.

Kolb, E.W. and Turner, M.S., “The Early Universe”, Reading, MA: Addison-Wesley Publishing Company, 1990.

Lamb, R.C., and Macomb, D.J., Ap. J. 488, 872, 1997.

Lynden-Bell, D., MNRAS 136, 101, 1967.

Mattox, J.R., et al. (EGRET collaboration), Ap. J. 461, 396, 1996.

McGaugh, S.S. and de Blok, W.J.G., Ap. J. 499, 41, 1998.

Merritt, D. and Cruz, F., Ap. J. Lett. 551, L41, 2001.

Metcalf, R., astro-ph/0109347.

Metcalf, R. Benton and Madau, P., Ap. J. 563, 9, 2001.

Milosavljević, M., Merritt, D., Rest, A., van den Bosch, F.C., astro-ph/0110185.

Moore, B., Calcáneo-Roldán, C., Stadel, J., Quinn, T., Lake, G., Ghigna, S., Governato, F., Phys. Rev. D 64, 63508, 2001.

Moore, B., Quinn, T., Governato, F., Stadel, J., Lake, G., MNRAS 310, 1147, 1999.

Morales, A., astro-ph/0112550.

Navarro, J.F., Frenk, C.S., and White, S.D.M., Ap. J. 462, 563, 1996.

Odenkirchen, M., et al. (SDSS), Astron. J. 122, 2538, 2001.

Pohl, M., Astron. Astrophys. 279, L17, 1993.

Power, C., Navarro, J.F., Jenkins, A., Frenk, C.S., White, S.D.M., Springel, V., Stadel, J., and Quinn, T., astro-ph/0201544.

Ravindranath, S., Ho, L.C., and Filippenko, A.V., Ap. J. 566, 801, 2002.

Rybicki, G.B. and Lightman, A.P., “Radiative Processes in Astrophysics”, New York, NY: John Wiley & Sons, 1979.

Schwarz, D.J., Hofmann, S., and Stöcker, H., astro-ph/0110601.

Serin, L., (ALEPH collaboration), hep-ex/0010049.

Sparke, L.S. and Gallagher, J.S., “Galaxies in the Universe”, Cambridge, UK: Cambridge University Press, 2000.

Sreekumar, P., et al. (EGRET collaboration), Ap. J. 494, 523, 1998.

Svensson, R., Ap. J. 258, 321, 1982.

van den Bergh, S., “The Galaxies of the Local Group”, Cambridge, UK: Cambridge University Press, 2000.

van den Bosch, F.C., Robertson, B.E., Dalcanton, J.J., and de Blok, W.J.G., Astron. J., 119, 1579, 2000.

van den Bosch, F.C. and Swaters, R.A., MNRAS 325, 1017, 2001.

Weekes, T.C. et al. (VERITAS collaboration), astro-ph/0108478; also see <http://veritas.sao.arizona.edu/veritas>.

Young, L.M., Astron. J., 117, 1758, 1999.